Classical dynamics of ionization, dissociation, and harmonic generation of a hydrogen molecular ion in intense laser fields: A collinear model

Yiwu Duan,[1,2] Wing-Ki Liu,[2] and Jian-Min Yuan[3]
[1]*Department of Physics, Hunan Normal University, Changsha, Hunan 410081, China*
[2]*Department of Physics, University of Waterloo, Waterloo, Ontario, Canada N2L 3G1*
[3]*Department of Physics and Atmospheric Science, Drexel University, Philadelphia, Pennsylvania 19104*
(Received 21 October 1998; revised manuscript received 11 November 1999; published 7 April 2000)

We use the classical trajectory method to study the dynamics of a hydrogen molecular ion interacting with intense laser fields employing a collinear model. We have calculated the probabilities of ionization and dissociation as functions of time and obtained the photoelectron and the nuclear fragmentation kinetic energy distribution spectra for various laser parameters. We have included a preliminary calculation of the harmonic generation spectra of a hydrogen molecular ion. In many cases, the classical results reproduce the qualitative features of the corresponding quantum-mechanical calculations.

PACS number(s): 33.80.Rv

I. INTRODUCTION

The development of high power femtosecond lasers have stimulated many studies of multiphoton phenomena in atoms and molecules [1–3]. Recently extensive quantum-mechanical calculations have been performed on the hydrogen molecular ion H_2^+ by numerically solving the time-dependent Schrödinger equation to obtain the ionization rates, dissociation probabilities, the kinetic energy spectra of the outgoing protons, and the harmonic generation spectra [4–8]. The H_2^+ was chosen because it is the simplest molecular ion, consisting of two protons and one electron. The exact three-body Hamiltonian with one-dimensional nuclear motion and three-dimensional electronic motion (1+3D) was employing in Refs. [5,6] using the usual absorbing boundary conditions to calculate the dissociation probabilities and ionization rates. To avoid the loss of information about the dynamics of the ionization and dissociation spectra, a wave-function splitting technique was developed to calculate the complete Coulomb explosion spectra, using a collinear model with one-dimensional nuclear and electronic motion (1+1D) [8]. This collinear model has recently been used to simulate the Coulomb explosion of H_2 under a 150 fs Ti:sapphire laser pulse, and agreement with experiment is found when the proper preparation of H_2^+ is taken into account [9]. An alternative quantum-mechanical approach employed the Floquet theory, resulting in a set of time-independent coupled equations [10–12], and together with the powerful technique of complex rotation, this method has been applied to the calculations of photodissociation rates [13] and harmonic generation [14] of H_2^+.

While quantum calculations, in principle, provide exact solutions to the multiphoton dynamics, they are computationally extremely demanding. On the other hand, classical trajectory calculation of the same problem, which is nonperturbative in nature, can readily be performed. Furthermore, classical analysis provides valuable insight into the dynamics of the systems, and often gives results in good agreement with quantum calculations. For atomic systems, classical mechanical studies of two-electron atoms showed that the bound-state motion exhibits both regular and chaotic dynamics [15,16]. The corresponding scattering problem of collinear electron-helium ion collisions has also been analyzed classically [17]. For molecular systems, Strand and Reinhardt [18] carried out a detailed analysis of the classical electronic motion of H_2^+ within the Born-Oppenheimer approximation (BOA), and showed that the BOA electronic surfaces using the uniform quantization conditions agree very well with the quantum results. The full dynamics of both the electronic and nuclear motion, beyond the BOA, has recently been studied [19–21].

Classical mechanics has been used routinely in the nonlinear dynamical analysis of multiphoton dissociation [22,23]. The response of atoms to strong laser fields has also been studied using classical mechanics. Examples include strong-field ionization [24–27], laser stabilization [28], and harmonic generation [29–32]. Recently, classical simulations of the ionization and dissociation of H_2^+ and multielectron diatomic molecules have been carried out [33,34].

In this paper, we study the classical dynamics of multiphoton ionization, dissociation, and harmonic generation by intense laser fields using a collinear 1+1D model for H_2^+ without making the Born-Oppenheimer approximation. This collinear model is expected to reproduce the essential features of a full 1+3D model at least qualitatively [7,33], and allows us to illustrate the details of the electron-nuclear dynamics clearly. A particular new feature in our work is that the initial conditions of our calculation is selected according to the semiclassical quantization of the initial state of the system. Furthermore, the kinetic energy spectra and the harmonic generation of H_2^+ are calculated classically.

We present our model in Sec. II and discuss the field-free dynamics of our system. The choice of initial conditions in our simulations is also described. In Sec. III, we present results of the ionization and dissociation of H_2^+ by lasers of wavelengths $\lambda = 300$ nm, 600 nm, and 900 nm, each at intensities of $I = 3.4\times10^{13}$, 2.1×10^{14}, and 8.5×10^{14} W/cm^2. The kinetic energy spectra of the ionized electrons and the nuclear fragments are discussed, and some preliminary re-

sults of harmonic generation are given. We summarize our results in Sec. IV.

II. MODEL

In this paper, we use a collinear model for the hydrogen molecular ion in which the electron and the two protons are restricted on a straight line. The Hamiltonian for the hydrogen molecular ion in an external intense laser is then given in atomic units by

$$H(R,P_R;x,p;t)=\frac{P_R^2}{2\mu_p}+\frac{p^2}{2\mu_e}+V_C(x,R)+V_{\rm ex}(x,t), \tag{1}$$

where R is the separation between the protons and P_R its conjugate momentum, x is the distance of the electron from the center-of-mass of the protons with p its conjugate momentum,

$$V_C(x,R)=\frac{1}{R}-\frac{1}{|x-R/2|}-\frac{1}{|x+R/2|}, \tag{2}$$

is the Coulomb interaction between the electron and the protons, and

$$V_{\rm ex}(x,t)=-\sigma x\mathcal{E}(t) \tag{3}$$

is the interaction potential with the external electric field $\mathcal{E}(t)$ of the laser. The reduced masses are $\mu_p=m_p/2$ and $\mu_e=2m_em_p/(2m_p+m_e)$, where m_p, $m_e(=1$ a.u.) are the proton and electron masses, respectively, and $\sigma=2(m_p+m_e)/(2m_p+m_e)$.

Hamilton's equations of motion can readily be obtained from Eq. (1). Because of the singularities of the bare Coulomb potential V_C whenever the electron collides with either proton, numerical integration becomes unstable. Such singularities can be removed by using the regularized coordinates [16]. Even though the regularized coordinates allow us to integrate the equations of motion numerically, with the bare Coulomb potential the electron is always trapped between the two protons if it is initially placed between them, and hence it cannot simulate the ionization process realistically. The usual remedy is to use a screened Coulomb potential [7,8,34,35]

$$V_{\rm sc}(x,R)=\frac{1}{R}-\frac{1}{\sqrt{(r-R/2)^2+q_e}}-\frac{1}{\sqrt{(r+R/2)^2+q_e}}, \tag{4}$$

with the justification that for large $|x|$, $V_{\rm sc}$ has the correct Coulomb behavior near the ionization threshold [35]. The parameter q_e is somewhat arbitrary, and in our study, we choose $q_e=0.1$ a.u. with reasons given below. No screening parameter is introduced in the Coulomb repulsion between the two protons since they never come close together in our study. We show in Fig. 1 the bare Coulomb potential V_C (solid curves) and the screened potential $V_{\rm sc}$ (dotted lines) with $q_e=0.1$ as functions of x for fixed values of R. It is clear that when the electron-proton separations are large, the two potentials are very similar. With the screened potential of Eq. (4), the Hamilton's equations for x, p, R, and P_R can be integrated numerically, using the fourth-order variable-step Runge-Kutta and the Bulirsch-Stoer methods [36].

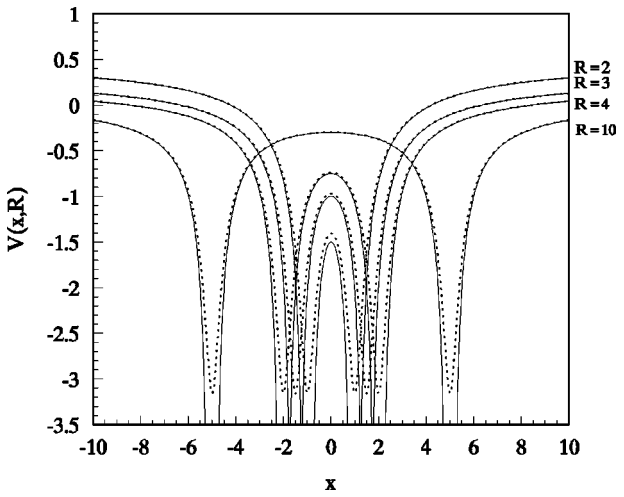

FIG. 1. Interation potential between the electron and the protons separated by R in H_2^+. Solid line: Coulomb potential of Eq. (2). Dotted lines: screened potential of Eq. (4) with $q_e=0.1$.

A. Classical dynamics in the field-free case

One advantage of using the collinear model is that its Poincaré surface of section (PSS) is only two dimensional. This fact facilitates the numerical study of its dynamical behavior in phase space. Details of the PSS can be found in Ref. [20] and will not be repeated here. We found that the PSS's for the screened potential were very similar to those for the bare Coulomb potential. For example, when the H_2^+ is in its ground vibrational state $v=0$, the center of the PSS for the screened potential at $R_0=3.182$ a.u. is very close to that for the bare Coulomb potential at $R_0=3.166$ a.u., and the region of the PSS at larger R is slightly distorted in the screened potential case. When the system is in its vibrationally excited state $v=6$, the PSS's for both the screened and the bare Coulomb potential consist of a stable Kolmogorov-Arnold-Moser (KAM) zone surrounded by another stable but irregular region, which is itself surrounded by an unstable region, in which the H_2^+ ion dissociates. The fact that the KAM zone is quasiperiodic and the surrounding region is chaotic is consistent with the results obtained from a Lyapunov exponent calculation [20].

The periodic orbit in the middle of the KAM zone turns out to be the antisymmetric stretching orbit, which is stable here, in contrast to that of atomic helium. The antisymmetric stretching periodic orbit corresponds to a periodic orbit in which the electron bounces between the two protons, and the distance R between the two protons remains almost constant. Using the classification scheme of Refs. [18–20], we can identify the trajectories inside the KAM zone as belonging to the P2 type. In this case, the electron bounces rapidly between the two protons, while the latter vibrate slowly relative to each other, making a breathing type of motion. An ex-

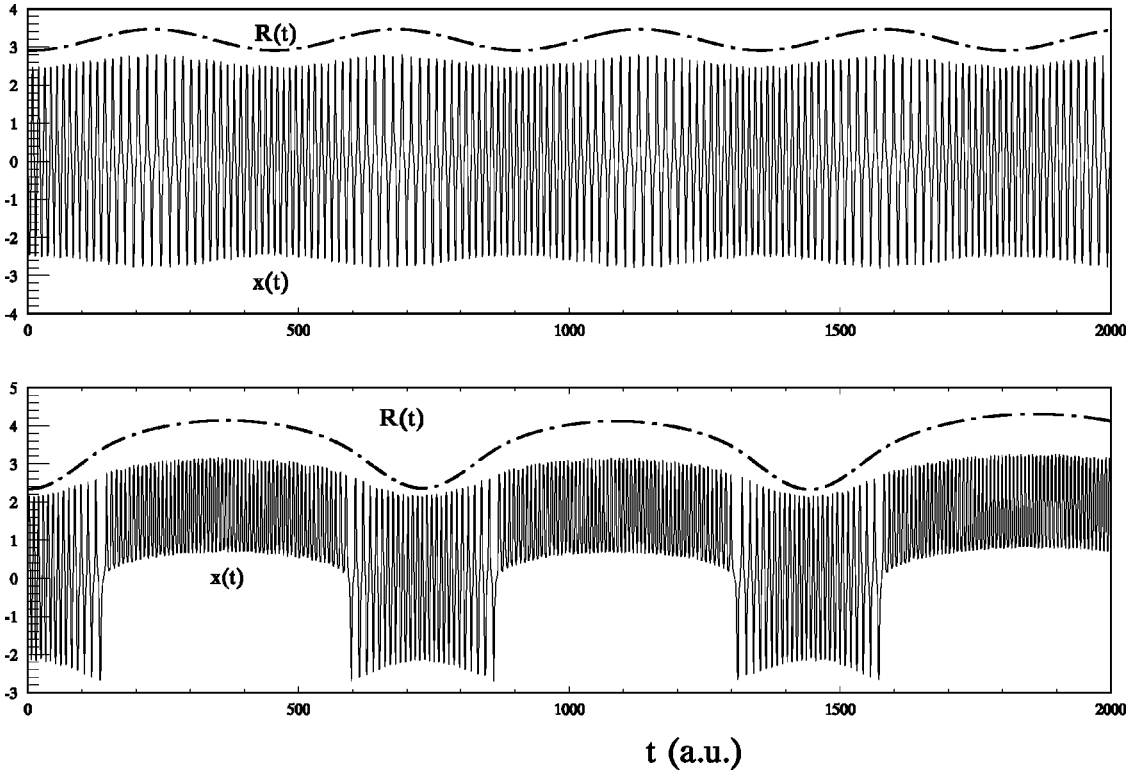

FIG. 2. Field-free trajectories using the screened potential. Solid lines: electronic coordinate $x(t)$, dot-dashed lines: nuclear separation $R(t)$. The upper trajectory is of the P2 type, while the lower one belongs to the P2/P3 hybrid motion.

ample of the P2 type of trajectory is shown in the upper plot of Fig. 2.

Another type of the trajectories shown in the lower plot of Fig. 2 is a one-dimensional equivalence of the P2/P3 hybrid motion [20]: it is clear from Fig. 1 that when the interproton distance is small, the potential barrier between two protons remains low, and the electron bounces between the two protons. As the interproton distance increases, the interproton barrier rises, and now the electron becomes trapped between one proton and the interproton barrier. This motion therefore represents a strong correlation between the nuclear and electronic motions and cannot be described adequately using the BOA, which ignores the proton motion. Although the P2/P3 hybrid motion is aperiodic, the motion is still bound and therefore represents a type of chemical bonding different from that of a P2 orbit. The fact that the net change of the interproton distance in the hybrid motion is much larger than that of the P2 type of motion suggests this to be a classical manifestation of the nonadiabatic electronic transition. Finally, we note that the transition from the regular to chaotic motion appears to be sudden and the correlation between the electron and nuclear motions is very similar to that between the light and heavy atoms in a heavy-light-heavy triatomic system [37,20].

B. The BOA and the initial conditions

In previous classical studies of multiphoton ionization and dissociation of molecules [33,34], the initial conditions were generated from a single trajectory in the field-free case at random time intervals. The justification is based on the ergodicity of the system. Study of the PSS shows that for small vibrational excitation, the phase space of the system is mostly quasiperiodic, and the proper initial conditions for quasi-classical calculations should be based on the semiclassical quantization conditions of the system [18,20,21]. How this can be done exactly remains to be solved; for our purpose, we propose to use the following approximate procedure based on the BOA, which is the semiclassical analog of the initial wave function used in Ref. [8].

We first solve for the electronic energy, treating the nuclear separation R as a parameter, for our collinear H_2^+ system using the bare Coulomb potential of Eq. (2). While the semiclassical method of Ref. [18] can be used, we have employed an exact quantum-mechanical procedure [38,39]. We then fit the ground-state potential to the Morse form

$$V_{\mathrm{Morse}}(R)=D(e^{-2\beta(R-b_0)}-2e^{-\beta(R-b_0)})-V_M, \qquad (5)$$

and obtain the parameters $D=0.3307$ a.u., $\beta=0.5$ a.u., $b_0=2.6$ a.u., and $V_M=0.5$ a.u. When the action-angle variables (I_{nu},Θ) are used, the total energy of the system in the electronic ground state

$$\frac{P_R^2}{2\mu_p}+V_{\mathrm{Morse}}(R)=E, \qquad (6)$$

takes the simple form $E=-D(1-I_{nu})^2-V_M$, where classically the action I_{nu} can take any value between 0 and 1 for the bound-state motion. The action-angle variables are related to (R,P_R) by [22]

$$R = b_0 + \frac{1}{\beta}\ln\left[\frac{1-\sqrt{1-\omega^2}\cos\Theta}{\omega^2}\right],$$
$$P_R = \sqrt{2\mu_p D}\frac{\omega\sqrt{1-\omega^2}\sin\Theta}{1-\sqrt{1-\omega^2}\cos\Theta}, \tag{7}$$

where $\omega = 1 - I_{nu}$. For a given nuclear vibration quantum number v, the action is given by the semiclassical quantization condition

$$I_{nu} = \left(v + \frac{1}{2}\right)\hbar_{\text{eff}}, \quad \hbar_{\text{eff}} = \frac{\hbar\beta}{\sqrt{2\mu_p D}}. \tag{8}$$

The angle Θ will be selected uniformly from 0 to 2π. Then each (I_{nu},Θ) will be substituted into Eq. (7) to obtain the initial values for (R,P_R).

After the nuclear separation and momentum are determined, we then consider the electronic Hamiltonian

$$H_{\text{el}}(x,p) = \frac{p^2}{2\mu_e} - \frac{1}{|x-R/2|} - \frac{1}{|x+R/2|} = E_{\text{el}}, \tag{9}$$

where $E_{\text{el}} = E - P_R^2/2\mu_p - 1/R$, and both P_R and R are treated as constants. The action-angle variables for the electronic motion under the BOA can now be calculated from

$$I_{\text{el}} = \frac{1}{2\pi}\oint p\,dx, \quad \theta = \frac{\partial}{\partial I_{\text{el}}}\int p\,dx = \int \frac{\partial p}{\partial H_{\text{el}}}\frac{\partial H_{\text{el}}}{\partial I_{\text{el}}}dx, \tag{10}$$

where from Eq. (9),

$$p(H_{\text{el}},x) = \pm\sqrt{2\mu_e\left(H_{\text{el}} + \frac{R}{(R/2)^2 - x^2}\right)}. \tag{11}$$

These action-angle variables can be expressed in term of the elliptic integrals

$$E(\kappa,\phi) = \int_0^\phi \sqrt{1-\kappa^2\sin\theta}\,d\theta,$$
$$F(\kappa,\phi) = \int_0^\phi \frac{d\theta}{\sqrt{1-\kappa^2\sin\theta}}, \quad \kappa^2 < 1. \tag{12}$$

Defining $k^2 = -E_{\text{el}}R/4$, it can be shown that $k^2 < 1$ corresponds to the P2-type motion in which the electron bounces between the two protons. In this case,

$$I_{\text{el}} = \frac{2\sqrt{2\mu_e R}}{\pi}E(k,\pi/2), \tag{13}$$

$$\theta = \frac{\pi}{2}\left(\frac{F(k,\alpha)-E(k,\alpha)}{F(k,\pi/2)-E(k,\pi/2)}\right), \tag{14}$$

where $x = (R/2)\cos\alpha$. On the other hand, if $k^2 > 1$, we have the P3-type motion where the electron oscillates between a proton and the internuclear barrier. Then

$$i = \frac{2\sqrt{2\mu_e R}}{\pi p}[E(p,\pi/2) - (1-p^2)F(p,\pi/2)], \tag{15}$$

$$\theta = \frac{\pi}{2}\left(\frac{F(p,\eta)-E(p,\eta)}{F(p,\pi/2)-E(p,\pi/2)}\right), \tag{16}$$

where $p = 1/k$ and $\sin\eta = k\sin\alpha$. For given E_{el}, the angle θ is chosen uniformly between 0 and π. Next Eq. (14) or (16) is inverted numerically to yield the corresponding values of α and hence x. Then Eq. (11) is used to give a pair of p of opposite signs, and we obtain a pair of initial conditions for the electron symmetric about the x axis in phase space.

Strictly speaking the above procedure applies only to the bare Coulomb potential case. As we note before, the dynamics of the system using the bare Coulomb potential and using the screened potential with $q_e = 0.1$ is quite similar, and the same procedure of choosing the initial conditions is applied to the latter case also. For the case of the screened potential with $v = 6$, a small fraction of the initial conditions gives rise to dissociation even in the absence of an external field. Such trajectories are not counted in the study of the interaction of intense laser field interaction with H_2^+ in the following sections. It should be emphasized that the BOA is used only in finding the initial conditions. Once these are determined, the full dynamics involving both the electronic and nuclear motion is considered, unless otherwise stated.

III. RESULTS AND INTERPRETATION

In this section, we present results of our classical trajectory calculation of the interaction of the laser with H_2^+. Hamilton's equations of motion for the Hamiltonian of Eq. (1) with the Coulomb potential V_C replaced by the screened potential of Eq. (4) are integrated numerically, with initial conditions chosen according to the procedure described in Sec. II B (see the discussion in the subsection on harmonic generation, however). The electric field of the laser pulse is represented by

$$\mathcal{E}(t) = \begin{cases} \mathcal{E}_0 \sin^2\dfrac{\pi t}{20T_0}\sin\omega_0 t, & 0 < t < 20T_0 \\ 0, \quad \text{otherwise}, \end{cases} \tag{17}$$

where $T_0 = 2\pi/\omega_0$ is the period of laser oscillation.

A. Ionization and dissociation

Under the action of an intense laser field, the electron of the H_2^+ may leave both nuclei, giving rise to ionization, or the two nuclei of the H_2^+ may separate from each other with positive relative velocity, and the ion dissociates. Following Ref. [34], we distinguish the following four dynamical processes:

(1) Survival: $R < 10$ a.u., $r_m < 20$ a.u.

(2) Ionization: $R < 10$ a.u., $r_m > 20$ a.u., and $dr_m/dt > 0$.

(3) Dissociation: $R > 10$ a.u., $dR/dt > 0$, and $r_m < 20$ a.u.

(4) Dissociative ionization: $R > 10$ a.u., $dR/dt > 0$, $r_m > 20$ a.u., and $dr_m/dt > 0$.

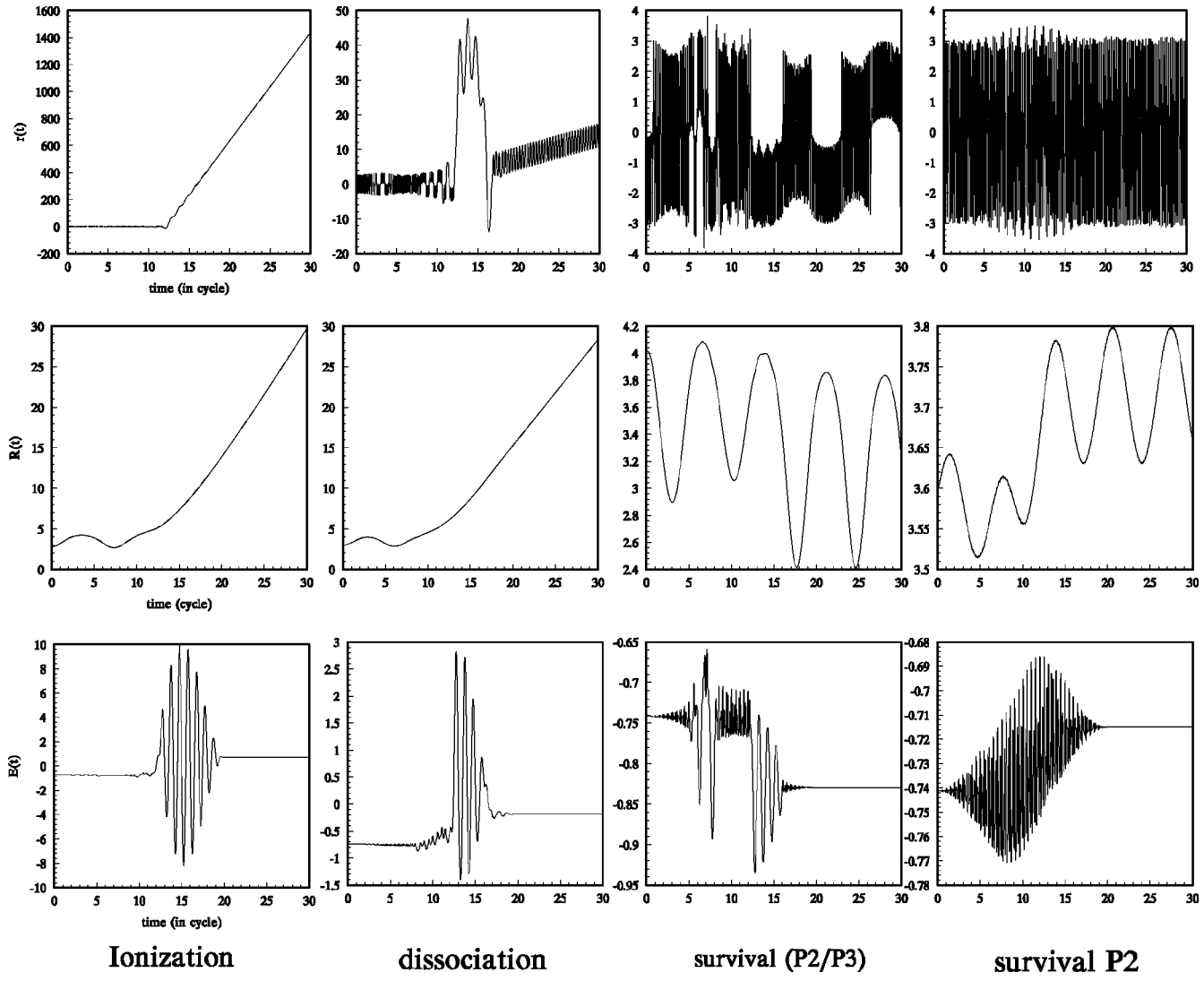

FIG. 3. Trajectories for different types of classical motion. $E(t)$ is the total energy given by the value of the Hamiltonian of Eq. (1) (with V_C replaced by V_{ex}) at time t.

Here $r_m=\min(|x-R/2|,|x+R/2|)$ is the separation of the electron from the closest proton of the H_2^+. The ionization process defined above is a transient process: eventually the nuclei will move apart due to Coulomb explosion, resulting in dissociative ionization.

In Fig. 3, we present trajectories illustrating these dynamical processes. The H_2^+ is initially in the $v=6$ vibrational level of the ground electronic state [6,8]. For ionization, we see that the electron leaves the nuclei rapidly when $t>12.5T_0$, while the nuclei drift apart much more slowly, reaching 10 a.u. at about $t\sim 15T_0$, after which the ion dissociates. As for the dissociation process, the electron can have large displacement from the center-of-mass of the protons in the duration of the laser pulse, but it comes back to stay near a proton as the H_2^+ ion dissociates into a hydrogen atom and a proton. This indicates that the dissociation process takes place via intermediate electronic excitation. The total energy of the system for both cases oscillates when the laser is turned on, and there is a net gain in energy after the passage of the laser pulse. When the H_2^+ remains bound after interacting with the laser, the system can lose or gain some energy and settle into the P2/P3 or P2 type of motion.

The probabilities of survival (P_s), ionization (P_i), dissociation (P_d), and dissociative ionization (P_{di}) when the H_2^+ is initially in the $v=6$ level are plotted in Fig. 4 for three different wavelengths of excitation (300, 600, and 900 nm) at high ($I=8.5\times 10^{14}$ W/cm^2) and moderate ($I=2.1\times 10^{14}$ W/cm^2) laser intensities. A total of 2400 trajectories are used to generate these probabilities. As expected, the survival probabilities decrease while P_i and P_{di} increase as the laser intensity increases. However, the dissociation probability P_d is not sensitive to I; in fact, for the shorter wavelength excitations, it becomes smaller at the higher laser intensity because ionization dominates. The dissociation process occurs earlier for the longer wavelength excitation; at the shortest wavelength of 300 nm, it appears when the laser pulse is almost over. At $I=2.1\times 10^{14}$ W/cm^2, P_d is slightly larger for the excitation wavelength of 300 nm, while at $I=8.5\times 10^{14}$ W/cm^2 it is the 900 nm laser that gives a slightly higher P_d.

In all cases that we studied, ionization occurs first, reaching a maximum in P_i within the duration of the laser pulse.

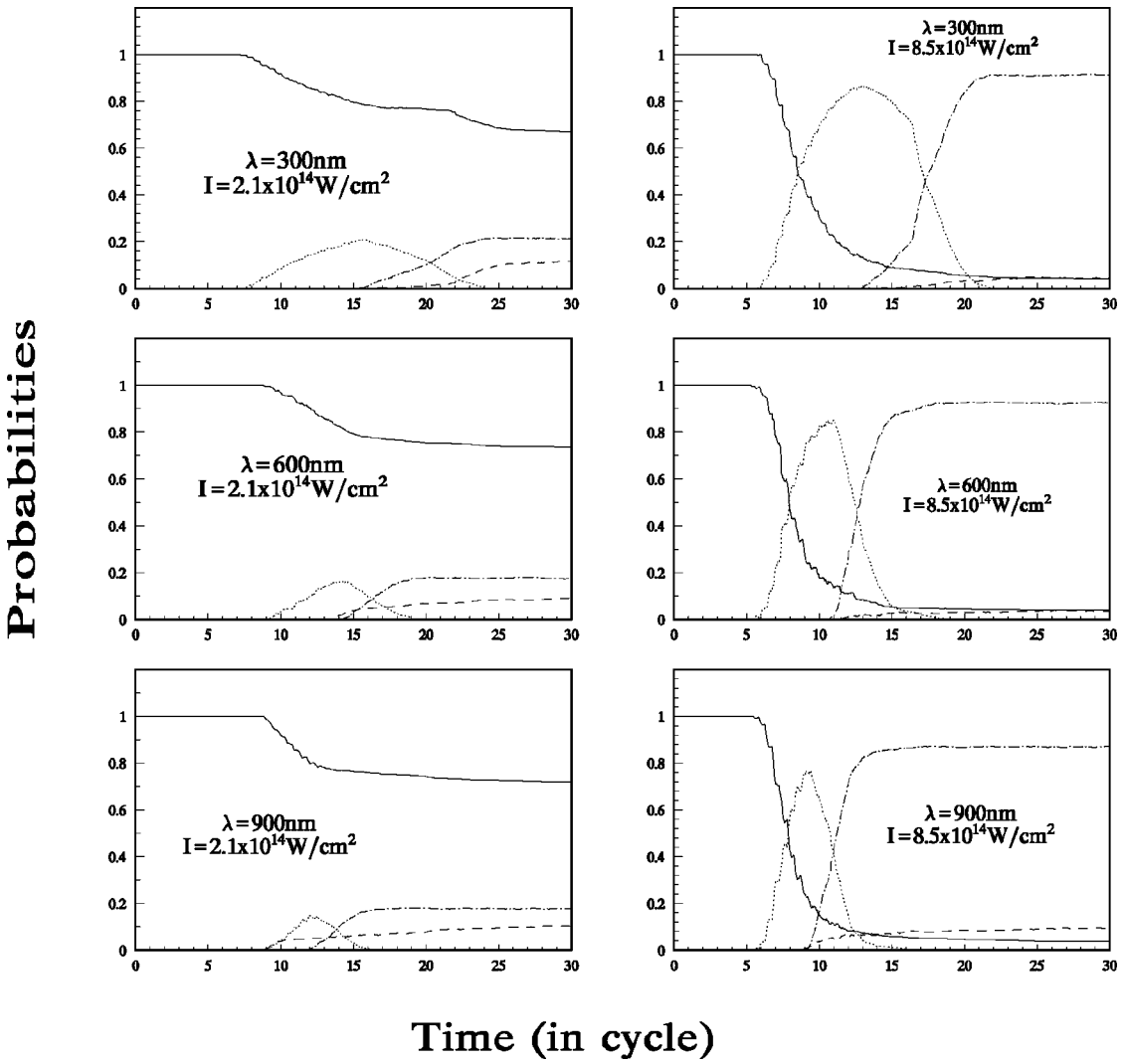

FIG. 4. The probabilities of survival (solid lines), dissociation (dashed lines), ionization (dotted lines), and dissociative ionization (dot-dashed lines) as functions of time. The H_2^+ is initially in the $v=6$ vibrational level.

For a fixed laser intensity, the peak of P_i occurs earlier for the longer wavelength excitation, while for the same laser wavelength, P_i peaks sooner at the higher laser intensity. P_i then decreases rapidly as the laser pulse cannot ionize any more H_2^+, and Coulomb explosion turns the process into dissociative ionization. At the same time, P_{di} appears as P_i begins to decrease from it peak value, and the gain in P_{di} can be observed to be about the same as the decrease in P_i. Hence virtually all the dissociative ionization events originate from the ionization process, and at least for the laser pulse we use, simultaneous ionization and dissociation of H_2^+, or subsequent ionization of the hydrogen atom after dissociation, seldom occurs. Our results are qualitatively similar to the quantum-mechanical calculations of Refs. [7,8] and the classical results of Ref. [34] where a 1+1D model of H_2^+ with different screening parameters and different laser characteristics were used. At the highest intensity ($I=10\times10^{14}$ W/cm^2) used in Ref. [34], however, P_d decreases slightly after reaching a peak, indicating some of the hydrogen atoms were ionized after dissociating from H_2^+.

When we lower the laser intensity to $I=3.4\times10^{13}$ W/cm^2, the ionization process stops, and only dissociation is observed (results not shown). At this intensity, P_d is larger for the longer wavelength excitation.

We have also studied these dynamical processes when the H_2^+ is initially in its ground vibrational level $v=0$ (results not shown). At the high laser intensity $I=8.5\times10^{14}$ W/cm^2, the results are very similar to those shown in Fig. 4, showing that the dynamics is not sensitive to the initial state of the molecular ion. At the lower intensity $I=2.1\times10^{14}$ W/cm^2, however, the values of P_d, P_i, and P_{di} are lower than those in Fig. 4, even though the qualitative features are similar. Thus at this lower intensity, initial vibrational excitation of the molecular ions helps to promote the ionization and dissociation processes.

B. Kinetic energy spectra

The classical trajectory method yields the electronic and nuclear kinetic energy distributions readily. In Fig. 5 we

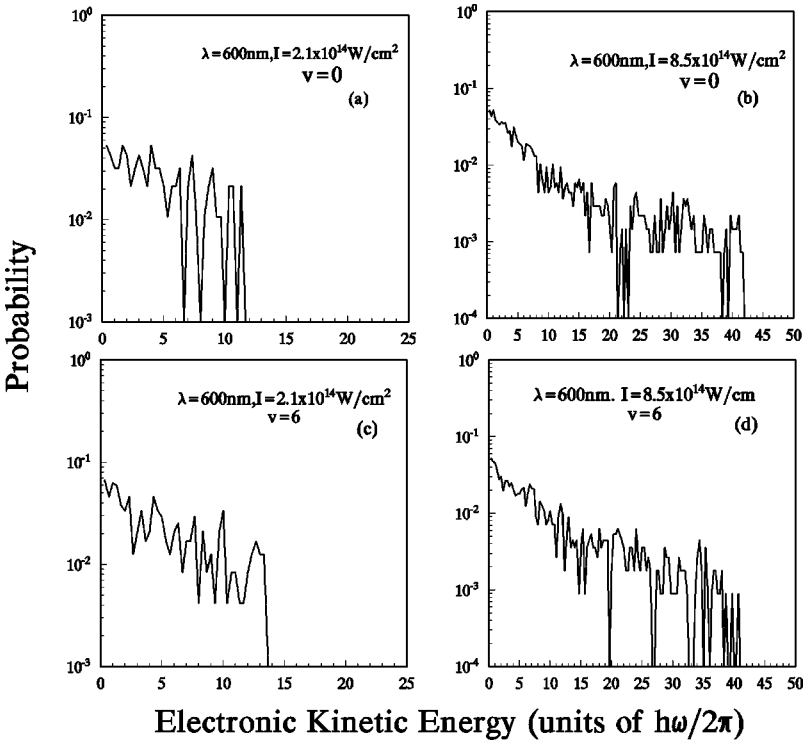

FIG. 5. The photoelectron kinetic energy spectra at the excitation wavelength $\lambda = 600$ nm. The electronic kinetic energy is measured in unit of the photon energy $\hbar\omega_0$.

present the photoelectron kinetic energy spectra for $\lambda = 600$ nm at two laser intensities, and compare the results for the H_2^+ in the initial vibrational levels $v = 0$ and $v = 6$. We use 4900 trajectories to generate these spectra. At the high intensity $I = 8.5 \times 10^{14}$ W/cm^2, the results between the $v = 0$ and $v = 6$ cases are qualitatively similar, while at the lower intensity $I = 2.1 \times 10^{14}$ W/cm^2, the ionization probability for $v = 0$ is smaller and has a lower energy cutoff value than the $v = 6$ case. Thus at the higher intensity, the H_2^+ can readily be ionized irrespective of its initial vibrational state. At the lower intensity, however, initial vibrational excitation of the H_2^+ enhances the ionization process.

At both intensities, the photoelectron spectra exhibit cutoff at the electronic kinetic energy of about $3U_p$, where $U_p = e^2E_0^2/4m_e\omega_0^2$ is the electron ponderomotive energy. (For $\lambda = 600$ nm, $U_p = 3.42\hbar\omega_0$ when $I = 2.1 \times 10^{14}$ W/cm^2, and $U_p = 13.83\hbar\omega_0$ when $I = 8.5 \times 10^{14}$ W/cm^2.) Recent quantum-mechanical calculation [8] also showed that the probability distribution dropped below 10^{-3} when the electron energy is larger than $3U_p$, but there was a second plateau which fell below 10^{-6} only when the electron energy is larger than $14U_p$. Because of the relatively small number of trajectories we use, we are not able to compute such small probabilities although, in principle, there is no inherent difficulty to increase the number of trajectories, except the demand of computer time.

In Fig. 6 we show the kinetic energy spectra of the dissociating nuclear fragments for $\lambda = 600$ nm and $\lambda = 900$ nm, at the laser intensities $I = 2.1 \times 10^{14}$ W/cm^2 and $I = 8.5 \times 10^{14}$ W/cm^2. We consider both the cases when the H_2^+ is initially in the $v = 0$ and the $v = 6$ vibrational levels. In all cases, the dissociation process $H_2^+ \rightarrow H + p$ contributes mainly to the low-energy part of the spectra, while the high-energy peaks are due to the Coulomb explosion process $H_2^+ \rightarrow p + p + e$. Furthermore, at the higher intensity, the Coulomb explosion process dominates over the dissociation process, and as expected, the high-energy peaks shift to higher energy compared with those at the lower laser intensity. This is consistent with the observation of Fig. 4. Figure 6(c) has the same qualitative features as those in Fig. 5(a) of the quantum results of Ref. [8], although the intensities used in the present study are higher. Note that there is a difference in scale between these figures. In our figures, we plot the probability density in units of probability per 0.1 eV.

At $\lambda = 600$ nm, with the laser intensity at the lower value of $I = 2.1 \times 10^{14}$ W/cm^2, the Coulomb explosion process gives rise to a more predominant fragmentation distribution when the H_2^+ is initially in its ground vibrational level, and very few dissociation events are observed. However, when the H_2^+ is initially in its $v = 6$ vibrational level, a sharp peak appears at lower energy, corresponding to the $H_2^+ \rightarrow H + p$ dissociation process, along with a broad distribution at high energy from Coulomb explosion. Hence under these excitation conditions, initial vibrational excitation enhances the dissociation process. At the higher laser intensity $I = 8.5 \times 10^{14}$ W/cm^2, the low-energy distributions from the dissociation process for both the $v = 0$ and the $v = 6$ cases are almost completely washed out, leaving broadened peaks at higher energies from the $H_2^+ \rightarrow p + p + e$ Coulomb explosion process.

When a laser with the longer wavelength of $\lambda = 900$ nm and the lower intensity of $I = 2.1 \times 10^{14}$ W/cm^2 is used to excite the H_2^+, a sharp peak due to $H_2^+ \rightarrow H + p$ appears at lower energy for both $v = 0$ and the $v = 6$ initial levels, although the peak intensity is slightly higher for $v = 6$. Again, broad peaks are observed at higher energies, and the quali-

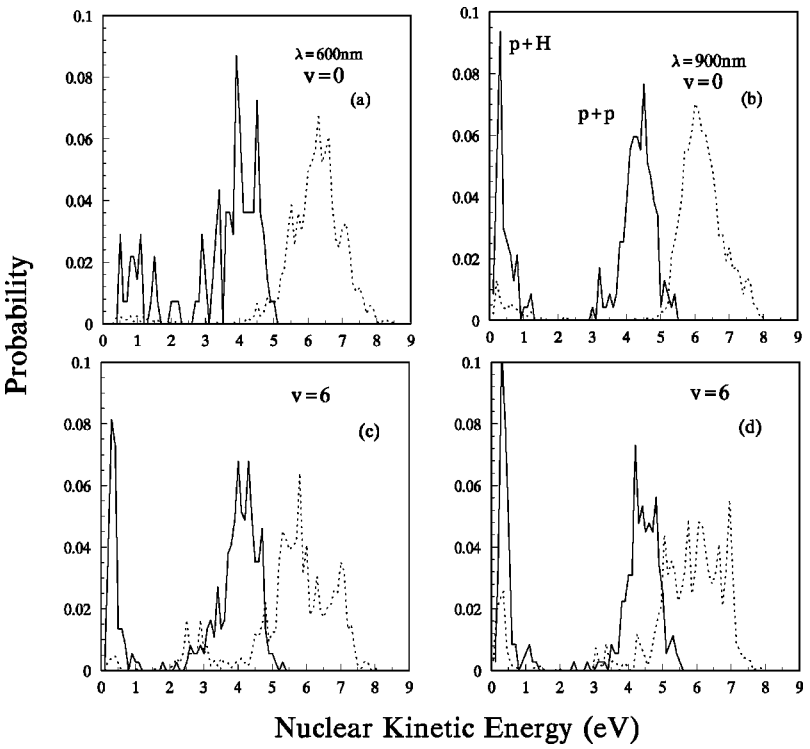

FIG. 6. Nuclear fragmentation spectra. Solid line: $I=2.1\times10^{14}$ W/cm^2; dotted line: $I=8.5\times10^{14}$W/cm^2.

tative features for these different initial states are quite similar. At the higher laser intensity, the $H_2^+\rightarrow H+p$ low-energy peaks are much suppressed, and the high-energy $H_2^+\rightarrow p+p+e$ peaks shift to higher energies and are broadened, especially for the $v=6$ case.

From Fig. 6, we can conclude that the strength of the low-energy dissociation peaks is very sensitive to the laser intensity, and also depends on the initial vibrational excitation, especially for $\lambda=600$ nm. The locations of both the low-energy $H_2^+\rightarrow H+p$ peaks and the high-energy $H_2^+\rightarrow p+p+e$ peaks are rather insensitive to the exciting wavelength. However, the locations of the higher energy peaks depend strongly on the laser intensity.

C. Harmonic generation

High-order harmonic generation under irradiation by high-intensity lasers has been observed for rare-gas atoms [40], and recently for molecular gases [3]. For the case of a hydrogen atom, the classical trajectory method proved to be a practical means for calculating the harmonic generation spectra [29]. This method can be applied to the present case of H_2^+.

Similar to the case of atomic hydrogen, the emission spectrum of H_2^+ is proportional to the power spectrum of the electronic dipole moment. From the classical trajectories, we can compute the Fourier transform of the average electron coordinate by the fast-Fourier transform method [36]

$$d(\omega)=\int_0^T\langle x(t)\rangle e^{i\omega t}dt, \tag{18}$$

where T is total time of integration, and $\langle\cdots\rangle$ represents an average over an ensemble of trajectories. The harmonic generation spectrum is then proportional to $|d(\omega)|^2$.

Experimentally, only the odd harmonics are observed in the emission spectra because of the inversion symmetry of the system. As pointed out in Refs. [29], even harmonics appears if we compute the power spectrum of a single trajectory since it does not possess an inversion center. The BOA initial conditions described in Sec. II B do not satisfy this symmetry requirement either, and hence the power spectrum of an ensemble average of $x(t)$ using these initial conditions will produce both odd and even harmonics. It has been emphasized in Refs. [29] that in order to remove the unphysical even harmonics, the inversion symmetry of the system must be built in from the initial conditions. Thus, instead of using the initial conditions of Sec. II B, we choose the initial nuclear coordinate and momentum to be $R=R_0$ and $P_R=0$. Then we use the same procedure described in Eqs. (10)–(14) to generate an ensemble of electronic initial conditions symmetric about $R=R_0$.

In Fig. 7, we show the ensemble-averaged electronic coordinates and their power spectra for $\lambda=900$ nm and $I=8.5\times10^{14}$ W/cm^2 and the H_2^+ at an initial energy corresponding to its ground vibrational level. Figures 7(a) and 7(c) are generated with the initial conditions described above and the full nuclear and electronic equations of motion are integrated numerically, while Figs. 7(b) and 7(d) are produced by freezing the nuclear separation at R_0, and only the electronic equations of motion are computed. 10 000 trajectories are employed in these calculations, and if the system ionizes, the ionizing part of the trajectory which would produce a dominant background [29], is excluded from the calculation of the spectrum. Note that at $t=0$, $\langle x(0)\rangle=0$ as required by the inversion symmetry. For the frozen-nuclei

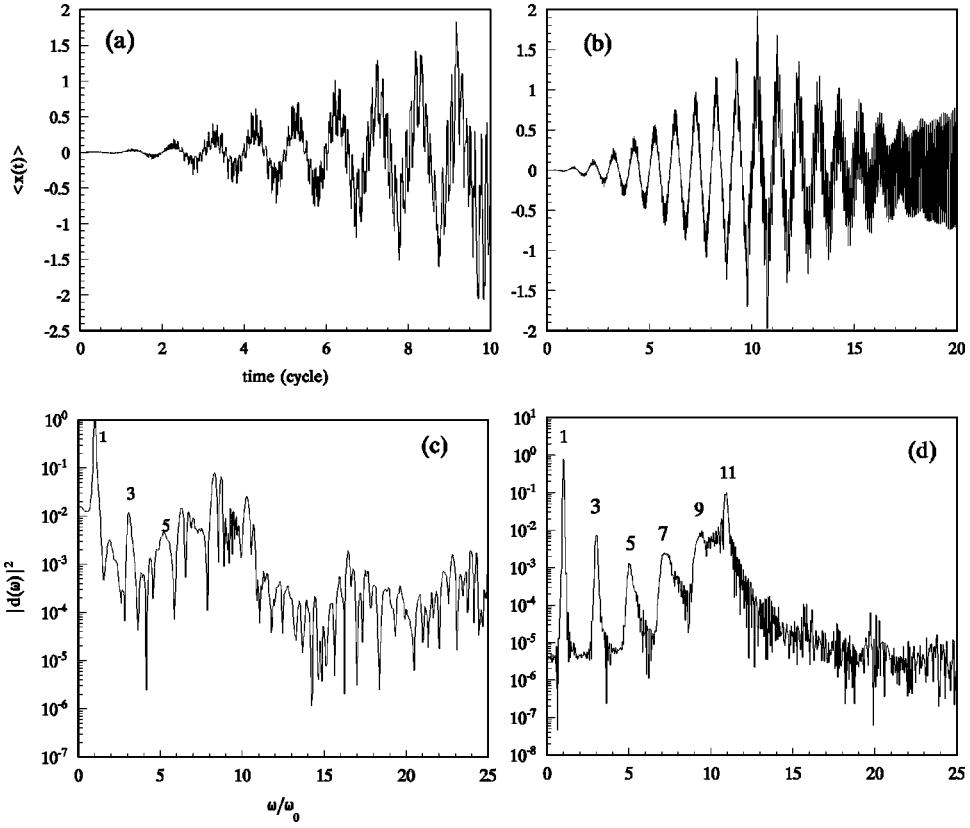

FIG. 7. Averaged electronic coordinates as functions of time [(a) and (b)], and the corresponding power spectra [(c) and (d)] in a laser with intensity $I=8.5\times10^{14}$ W/cm^2. (a) and (c): full nuclear and electronic dynamics; (b) and (d): nuclear separation frozen at R_0, the center of the Poincaré surface of section.

case, lower order even harmonics are suppressed, and odd harmonics of up to the 11th order can be observed. The power spectrum using the full dynamics is much noiser, and only up to the fifth-order odd harmonics is distinguishable. We have also computed the spectra at the lower intensity of $I=3.4\times10^{13}$ W/cm^2 (not shown). Again, odd harmonics of lower orders readily appear in the frozen-nuclei case, but the spectrum from the full dynamics is even noisier.

Our results are less satisfactory than those of atomic hydrogen [29] since only a few of the lower-order odd harmonics are generated. Experimental [3] and quantum-mechanical calculation [4,6] indicated high-order odd harmonics are emitted from molecules interacting with intense laser pulses. The initial conditions we choose is *ad hoc* even though they satisfy the inversion symmetry requirement. The spectra of the frozen-nuclei case may not be too meaningful physically, especially for high-intensity excitation where considerable dissociation occurs, but are included to illustrate the importance of using an ensemble with the proper inversion symmetry. Further work on the classical calculation of molecular harmonic generation remains to be done.

IV. SUMMARY AND CONCLUSION

In this paper, we have presented a classical trajectory study of the dynamical processes when a hydrogen molecular ion interacts with intense laser fields. A collinear model of H_2^+ is used, with the bare Coulomb potential replaced by a screened potential to avoid the singularities at close electron-proton encounters. The collinear model has the advantage that the phase-space dynamics in the field-free case can be conveniently analyzed in terms of the two-dimensional Poincaré surfaces of section. Since the motion of the low-lying states of the H_2^+ is quasiperiodic, initial conditions based on the ergodic hypothesis may not be sufficient to properly characterize the initial quantum state of the system in the classical trajectory simulation. Hence we propose an approximate semiclassical procedure based on the Born-Oppenheimer approximation and using action-angle variables to choose the initial conditions for the trajectory calculations.

During the interaction with the laser field, the electronic and nuclear motion becomes strongly coupled, and we have studied the probabilities of ionization, dissociation, dissociative ionization, and survival as a function of the laser characteristics as well as the initial states of the H_2^+. As expected, the ionization and dissociative ionization probabilities increase with increasing laser intensity, but the dissociation probability is not sensitive to the laser intensity. The peak of the ionization process occurs sooner for longer laser wavelength and higher laser intensity. Once ionized, the nuclei (protons) of the H_2^+ will eventually fly apart by Coulomb explosion. We find almost all the dissociative ionization events come from Coulomb explosion, indicating that simultaneous ionization and dissociation, or subsequent ionization of the hydrogen atom after dissociation, is highly unlikely. By comparing the results for the H_2^+ initially at the $v=0$ and the $v=6$ levels, we conclude that initial vibrational excitation enhances the ionization and dissociation processes only at the lower laser intensity. The qualitative behavior of these probabilities is very similar to those from

quantum-mechanical calculations.

We have calculated the photoelectron kinetic energy distributions, and found that there is a cutoff at an energy of about $3U_p$ where U_p is the ponderomotive energy. Due to the relative small number of trajectories used, we cannot detect a second plateau in the spectra which were observed in quantum-mechanical calculations. We have also studied the energy spectra of the dissociating nuclear fragments, and found that the dissociating process $H_2^+ \rightarrow H + p$ gives rise to a low-energy sharp peak, while the Coulomb explosion $H_2^+ \rightarrow p + p + e$ produces broad high-energy peaks. At the lower intensity, both the low-energy dissociation peak and the high-energy Coulomb explosion peaks are clearly displayed, but at high laser intensity, the Coulomb explosion peaks become dominant, broadened, and shifted to higher energy.

Finally, we have carried out a preliminary classical calculation of the harmonic generation spectra of H_2^+. In order to suppress the unphysical even harmonics, the initial conditions must satisfy the inversion symmetry of the system, and we have introduced an *ad hoc* procedure for the choice of the initial conditions. While the spectra generated under the frozen-nuclei condition produces odd harmonics up to order 11, only a few odd harmonics show up in the spectra when the full nuclear and electronic dynamics is included, in contrast to experimental finding and quantum-mechanical calculations.

We believe that the initial conditions based on the BOA should be a reliable procedure for low-lying states of the H_2^+ since quantum-mechanical calculations based on the BOA agree very well with experiments [41]. In addition, we have used the electronic ground-state potential readily available to us for the bare Coulomb potential to generate initial conditions which are subsequently used for the model H_2^+ with the screened potential. This last approximation is not essential but is done for expediency. Our present procedure is reasonable as long as the screening parameter, which we choose to be $q_e = 0.1$, is small, and as already discussed, our ionization and dissociation results agree qualitatively with quantum calculations.

However, our procedure for choosing the initial conditions, or perhaps any procedure that depends on the BOA, may not be adequate for the calculation of harmonic generation, as suggested by the results of Sec. III C. We believe that the proper initial conditions based on the semiclassical quantization of the full electron-nuclei dynamics of H_2^+, with the proper inversion symmetry built-in, are required for accurate calculation of the harmonic generation spectra. Work on such semiclassical quantization has appeared recently [19–21], and we are considering various methods to implement these ideas for the spectral calculation. Finally, it should be mentioned that while quantum-mechanical calculations based on the 1+1D model are in reasonable agreement with experiments when proper initial conditions are used, for quantitative comparison a full three-dimensional study should be carried out. Work on higher dimensional models is in progress.

ACKNOWLEDGMENTS

This work is partially supported by Grant No. 19874019 from the National Natural Science Foundation of China (Y.W.D.) and a research grant from the Natural Sciences and Engineering Research Council (NSERC) of Canada (W.K.L.). J.M.Y. would like to acknowledge the partial support by the National Science Foundation through a grant for the Institute for Theoretical Atomic and Molecular Physics at Harvard University and Smithsonian Astrophysical Observatory. W.K.L. would like to thank the Institute of Atomic and Molecular Sciences, Academia Sinica, Taipei, and Hunan Normal University for their hospitality during his visits when part of this work was undertaken.

[1] P. B. Corkum and P. Dietrich, Comments At. Mol. Phys. **28**, 357 (1993).
[2] *Molecules in Laser Fields*, edited by A. D. Bandrauk (Marcel Dekker, New York, 1994).
[3] Y. Liang, S. Augst, S. L. Chin, Y. Beaudoin, and M. Chaker, J. Phys. B **27**, 5119 (1994); Y. Liang, S. Augst, Y. Beaudoin, M. Chaker, H. Yu, A. D. Bandrauk, and S. L. Chin, *ibid.* **28**, 3661 (1995).
[4] T. Zuo, S. Chelkowski, and A. D. Bandrauk, Phys. Rev. A **48**, 3837 (1993).
[5] S. Chelkowski, T. Zuo, O. Atabek, and A. D. Bandrauk, Phys. Rev. A **52**, 2977 (1995).
[6] S. Chelkowski, A. Conjusteau, T. Zuo, and A. D. Bandrauk, Phys. Rev. A **54**, 3235 (1996).
[7] K. C. Kulander, F. H. Mies, and K. J. Schafer, Phys. Rev. A **53**, 2562 (1996).
[8] S. Chelkowski, C. Foisy, and A. D. Bandrauk, Phys. Rev. A **57**, 1176 (1998).
[9] T. D. G. Walsh, F. A. Ilkov, S. L. Chin, F. Châteauneuf, T. T. Nguyen-Dang, S. Chelkowski, A. D. Bandrauk, and O. Atabek, Phys. Rev. A **58**, 3922 (1998).
[10] S. I. Chu, J. Chem. Phys. **75**, 2215 (1981).
[11] J. Shertzer, A. Chandler, and M. Gavrila, Phys. Rev. Lett. **73**, 2039 (1995).
[12] M. Gavrila and J. Shertzer, Phys. Rev. A **53**, 3431 (1996).
[13] M. Chrysos, O. Atabek, and R. Lefebvre, Phys. Rev. A **48**, 3845 (1993); **48**, 3855 (1993).
[14] N. Moiseyev, M. Chrysos, O. Atabek, and R. Lefebvre, J. Phys. B **28**, 2007 (1995).
[15] R. Blumel and W. R. Reinhardt, in *Quantum Nonintegrability: Directions in Chaos*, edited by D. H. Feng and J.-M. Yuan (World Scientific, Singapore, 1992), Vol. 4, p. 254.
[16] K. Richter, G. Tanner, and D. Wintgen, Phys. Rev. A **48**, 4182 (1993).
[17] X. Tang, Y. Gu, and J.-M. Yuan, Phys. Rev. A **54**, 496 (1996).
[18] M. P. Strand and W. P. Reinhardt, J. Chem. Phys. **70**, 3812 (1979).
[19] Y. W. Duan, J. M. Yuan, and C. G. Bao, Phys. Rev. A **52**, 3497 (1995).

[20] Y. W. Duan, C. Browne, and J. M. Yuan, Phys. Rev. A **59**, 238 (1999).
[21] J. Mueller, J. Burgdoerfer, and D. W. Noid, J. Chem. Phys. **103**, 4985 (1995); K. Sohlberg, R. E. Tuzun, B. G. Sumpter, and D. W. Noid, Phys. Rev. A **57**, 906 (1998).
[22] Y. Gu and J.-M. Yuan, Phys. Rev. A **36**, 3788 (1987).
[23] V. Constantoudis and C. A. Nicolaides, Phys. Rev. A **55**, 1325 (1997).
[24] S.-I Chu and R. Y. Yin, J. Opt. Soc. Am. B **4**, 720 (1987).
[25] G. A. Kyrala, J. Opt. Soc. Am. B **4**, 731 (1987).
[26] J. Grochmalick, J. Mostowski, and M. Trippenbach, J. Phys. B **21**, 1673 (1988).
[27] D. A. Wasson and S. E. Koonin, Phys. Rev. A **39**, 5676 (1989).
[28] M. Gajda, J. Grochmalicki, M. Lewenstein, and K. Rzążewski, Phys. Rev. A **46**, 1638 (1992); K. Rzążewski, M. Lewenstein, and P. Saliéres, *ibid.* **49**, 1196 (1994).
[29] G. Bandarage, A. Maquet, and J. Cooper, Phys. Rev. A **41**, 1744 (1990); G. Bandarage, A. Maquet, T. Ménis, R. Taïeb, V. Véniard, and J. Cooper, *ibid.* **46**, 380 (1992).
[30] P. B. Corkum, Phys. Rev. Lett. **71**, 1994 (1993).
[31] S.-I Chu, K. Wang, and E. Layton, J. Opt. Soc. Am. B **7**, 425 (1990).
[32] V. Averbukh and N. Moiseyev, Phys. Rev. A **57**, 1345 (1998).
[33] D. M. Villeneuve, M. Yu. Ivanov, and P. B. Corkum, Phys. Rev. A **54**, 736 (1996).
[34] W. Qu, S. Hu, and Z. Xu, Phys. Rev. A **57**, 2219 (1998); **57**, 4528 (1998).
[35] J. H. Eberly, Q. Su, and J. Javanainen, J. Opt. Soc. Am. B **6**, 1289 (1989).
[36] W. H. Press, S. A. Teukolsky, W. T. Vetterling, and B. P. Flannery, *Numerical Recipes*, 2nd ed. (Cambridge University Press, Cambridge, 1992).
[37] R. Skodje and M. J. Davis, J. Chem. Phys. **88**, 2429 (1988).
[38] Y. Duan, M. Yin, W. An, and C. He, Commun. Math. Phys. **31**, 27 (1998).
[39] D. Rapp, *Quantum Mechanics* (Holt, Rinehard and Winston, New York, 1971), pp. 366–367.
[40] A. L'Huillier, K. J. Schafer, and K. C. Kulander, J. Phys. B **24**, 3115 (1991), and references therein.
[41] C. A. Leach and R. E. Moss, Annu. Rev. Phys. Chem. **46**, 55 (1995).